Batch Removal of Aqueous Cu^{2+} Ions Using Nanoparticles of Zero-Valent Iron: A Study of the Capacity and Mechanism of Uptake

Duygu Karabelli,[†] Çağrı Üzüm,[†] Talal Shahwan,*[,†] Ahmet E. Eroğlu,[†] Tom B. Scott,[‡] Keith R. Hallam,[‡] and Ingo Lieberwirth[§]

Department of Chemistry, İzmir Institute of Technology, Urla 35430, İzmir, Turkey; Interface Analysis Centre, University of Bristol, 121 St Michael's Hill, Bristol BS2 8BS, England; and Max Planck Institute for Polymer Research, Mainz, Germany

In this study, nZVI prepared by borohydride reduction was applied for the removal of Cu^{2+} ions under a variety of experimental conditions. The uptake experiments investigated the effects of initial concentration, contact time, pH, and repetitive loading on the extent of retardation of Cu^{2+} ions. Within the applied conditions, the sorbent demonstrated fast uptake kinetics and outstanding fixation abilities up to an initial Cu^{2+} concentration of 200.0 mg/L. Partitioning of Cu^{2+} ions between liquid and solid phases demonstrated an isotherm of L-type. Within the studied conditions, the capacity of uptake was found to be 250 mg of Cu^{2+} per g of nZVI. According to X-ray photoelectron spectroscopy (XPS) and X-ray diffraction (XRD) results, Cu^{2+} ions were sorbed primarily via a redox mechanism that resulted in the formation of Cu_2O and Cu^0. The contact of iron nanoparticles with aqueous media caused extensive formation of iron oxide. However, the material did not completely lose its removal capacity and was repeatedly applied at low concentrations for further uptake trials.

1. Introduction

Nanosized zerovalent iron (nZVI) technology is seen as one of the most prominent, rapidly emerging environmental technologies with considerable potential benefits.[1] This technology could provide cost-effective solutions to some of the most challenging environmental cleanup problems.[2] The application of this technology is offering the advantage of easier delivery to deep contamination zones and larger surface reactivity in comparison to scrap Fe^0 used in conventional permeable reactive barriers.[3] In addition to the enormous amount of energy stemming from their high surface/volume ratios, iron nanoparticles provide a kinetic advantage in the uptake process.[4] In spite of some still unresolved uncertainties associated with the application of iron nanoparticles, this material is being accepted as a versatile tool for the remediation of different types of contaminants in groundwater, soil, and air on both the experimental and field scales.[5] The application of iron nanoparticles for the removal of different types of aqueous metal ions is a growing subject. The fixation capacity of nZVI and mechanism of interaction of this material with various metal ions have been investigated in a number of previous works.[6–12]

Heavy metals are continuously discharged into the environment as a result of various kinds of anthropogenic activities. Copper is one of the most common pollutants in industrial effluents, among which are those of power stations, electroplating, combustion, mining, and smelting.[13] This element is an essential trace element for living organisms, but its intake at high levels can cause detrimental health effects. On the basis of its toxicity and persistent characteristics, copper is reported to be among the priority elements when groundwater-associated runoff problems are addressed.[14]

In previous studies, cast iron grit mixed with silica sand was applied in column experiments for the removal of aqueous Cu^{2+} ions.[13] In another study, zerovalent iron in the scrap form was tested previously for the uptake of aqueous Cu^{2+} ions.[14] The mechanism of uptake of different ions, including Cu^{2+}, by nZVI has been investigated, and the fixation of Cu^{2+} was attributed to a redox mechanism that leads to Cu^0 formation.[9] To our knowledge, this study represents the first attempt to study the removal of Cu^{2+} ions by nZVI under different experimental conditions.

This work encompasses determining the effects of concentration, time, pH, and repetitive loading on the extent of Cu^{2+} retardation by nZVI. Flame atomic absorption spectrometry (FAAS) was used to determine the aqueous concentration of copper ions. The sorbent materials were characterized using scanning electron microscopy/energy dispersive X-ray analysis (SEM/EDX), high-resolution−transmission electron microscopy (HR-TEM), X-ray photoelectron spectroscopy (XPS), and X-ray diffraction (XRD).

2. Experimental Section

2.1. Preparation of nZVI. The synthesis of nZVI can be realizable using a variety of physical and chemical synthesis techniques. A summary of these techniques was presented in a review paper on the topic by Li et al.[5] In this study, nZVI was synthesized using the method of liquid-phase reduction utilizing sodium borohydride as the reducing agent. The applied procedure was based in part on a previously reported one[15] and was given also in detail in earlier studies carried out at our laboratories.[11,12] A 17.8 g sample of $FeCl_2 \cdot 4H_2O$ was dissolved first in 50.0 mL of solution of absolute ethanol and distilled water (4:1 v/v). Meanwhile, 8.47 g of $NaBH_4$ was separately dissolved in 220 mL of distilled water to have ~1 M solution. $NaBH_4$ solution was then added to Fe^{2+} solution dropwise (40−50 drops/min) while providing stirring to the reaction mixture. The black particles of nZVI appeared immediately after introducing the first drops of $NaBH_4$ solution, and the solution was mixed for an extra 20 min after the addition of all the $NaBH_4$ solution. The iron powder was then separated from

* Corresponding author. E-mail: talalshahwan@iyte.edu.tr. Tel.: 90 232 750 7540. Fax: 90 232 750 7509.
[†] İzmir Institute of Technology.
[‡] University of Bristol.
[§] Max Planck Institute for Polymer Research.

10.1021/ie800081s CCC: $40.75
Published on Web 06/20/2008

Table 1. Measured pH Values at the Start and End of Mixing of nZVI with Cu^{2+} Solutions at Different Initial Concentrations; In Each Experiment, 50.0 mL of Each Cu^{2+} Solution Were Mixed With 0.050 g of the Adsorbent

initial concentration (mg/L)	initial pH	final pH
10.0	8.09	4.09
50.0	6.51	3.68
100.0	5.21	3.48
250.0	4.75	3.20
500.0	4.67	3.15

Table 2. Amounts of Cu^{2+} Fixed By Different Doses of nZVI at the Initial Cu^{2+} Concentration of 500.0 mg/L

nZVI (g)	$[Cu]_l$ (mg/L)	$[Cu]_s$ (mg/g)	% uptake
0.050	284	216	43.3
0.075	260	240	48.0
0.100	198	302	60.4
0.150	<0.1	>499.9	>99.9

Table 3. Comparison of Cu^{2+} Uptake Capacities By Different Sorbent Materials

sorbent	uptake capacity (mg/g)	reference
nZVI	250	this study[a]
ZVI/sand mixture	13.3	13
Fe_3O_4 nanoparticles with gum arabic	38.5	18
functionalized polymer-coated silica gel	76.33	19
grafted silica	16.5	20
activated slag	30.0	21
wheat bran	15.0	22
Spirogyra species	133.3	23

[a] Estimated from the isotherm in Figure 4.

Table 4. Composition of the Simulated Industrial Estate Wastewater Used in This Study

chemical species	concentration (mg/L)
Zn^{2+}	20.0
Cu^{2+}	20.0
glucose	1437.5
urea	107.3
$FeSO_4 \cdot 7H_2O$	24.8
KH_2PO_4	43.8
pH 6.5	

solution using vacuum filtration. The filtrate was washed at least three times with 99% absolute ethanol. The powder was finally dried at 75 °C overnight. The drying step was performed in the oven without air evacuation, as drying in an evacuated oven caused the sample to spontaneously ignite upon exposure to atmospheric oxygen.

2.2. Uptake Experiments. The solutions of copper ions were prepared from $Cu(NO_3)_2 \cdot {}^5/_2H_2O$ salt dissolved in ultrapure water (18 MΩ). The initial concentrations used in the uptake experiments included 10.0, 50.0, 100.0, 200.0, 400.0, and 500.0 mg/L, which were prepared by serial dilution from a 1000.0 mg/L stock Cu^{2+} solution.

The kinetic aspect of the uptake process was studied at the initial Cu^{2+} concentrations of 100.0 and 500.0 mg/L. In each experiment, 50.0 mL portions of Cu^{2+} solution were mixed with 0.050 g of nZVI. The solutions were shaken in a water bath for the periods of 1 min, 5 min, 10 min, 30 min, 1 h, 2 h, 4 h, 7 h, 16 h, and 24 h. The liquid was then separated from the solid by centrifugation followed by filtration.

In order to study the effect of concentration on the extent of removal of Cu^{2+} by nZVI, 50.0 mL of each Cu^{2+} solution with initial concentrations of 10.0−500.0 mg/L were mixed with 0.050 g of the adsorbent. The solutions were shaken at room temperature for 4 h.

Table 5. Elemental Concentrations (mg/L) of Ca, Mg, Cu, and Fe Obtained From ICP-AES Measurements

initial conc. of Cu^{2+} (mg/L)	elemental content at the end of uptake (mg/L)			
	Cu	Ca	Mg	Fe
10.0	0.0	78.7	10.1	3.9
25.0	0.0	75.2	9.9	4.9
50.0	0.0	73.0	10.0	0.8
75.0	0.0	77.1	10.1	0.8
100.0	0.3	82.6	10.0	0.7

The effect of the applied dose of the adsorbent on the extent of uptake was studied for the initial Cu^{2+} concentration of 500.0 mg/L. In this part, 0.050, 0.075, 0.10, and 0.15 g doses of the adsorbent were mixed with 50.0 mL aliquots of Cu^{2+} solution and were shaken for 4 h.

The effect of successive applications on the reactivity of the adsorbent was studied at the initial concentrations of 10.0 and 100.0 mg/L. For this purpose, 50.0 mL portions of Cu^{2+} solution were mixed with 0.050 g of the adsorbents and shaken for 1 h at room temperature. The mixture was then centrifuged, and the Cu-loaded iron sample was exposed again to another 50 mL portion of fresh Cu^{2+} solution. The process was repeated for six successive trials.

The effect of pH adjustment on Cu^{2+} uptake was studied at the initial concentration of 50.0 mg/L. In these experiments, 50.0 mL aliquots of Cu^{2+} solution were mixed with 0.050 g of the adsorbent for 1 h at room temperature. The pH was adjusted at the start of mixing to 3.0, 5.0, 7.0, 9.0, and 11.0, using 0.1 N HCl or NaOH solutions.

2.3. Characterization Techniques. Throughout this study, the solutions were mixed with nZVI samples placed in 50 mL polypropylene centrifuge tubes using a lateral shaker. The liquid phase was analyzed using a Thermo Elemental SOLAAR M6 series atomic absorption spectrometer with air−acetylene flame. The solid samples were characterized using XPS, XRD, HR-TEM, and SEM/EDX.

During the XPS analysis, the samples were mounted in Al holders and analyzed under high vacuum ($<1 \times 10^{-7}$ mbar) in a Thermo Fisher Scientific Escascope X-ray photoelectron spectrometer equipped with a dual anode. Al Kα radiation was used at 400W (15 kV) for the analyses. Data analysis was carried out using Pisces (Dayta Systems, U.K.) software.

A Philips X'Pert Pro instrument was used for the XRD analysis. The source consisted of Cu Kα radiation ($\lambda = 1.54$ Å). SEM/EDX analysis was carried out using a Philips XL-30S FEG type instrument. The solid samples were sprinkled onto adhesive carbon tapes supported on metallic disks.

HR-TEM analysis was performed using a Tecnai F20. The instrument was operated at 200 kV acceleration voltage. Prior to analysis, the nZVI sample was dispersed in ethanol using an ultrasonic bath. Subsequently, a drop of the dispersion was applied to a holey carbon transmission electron microscopy (TEM) support grid, and excess solution was blotted off by a filter paper.

3. Results and Discussion

3.1. Speciation Analysis. In aqueous solution, copper can assume different chemical forms that depend on the pH of the medium. The speciation analysis of aqueous copper ions was performed using visual MINTEQ software at various input conditions of initial concentration, temperature, pH, and ionic strength values. The obtained results indicated that, up to the pH value of 6.5, copper will exist in solution mainly in its

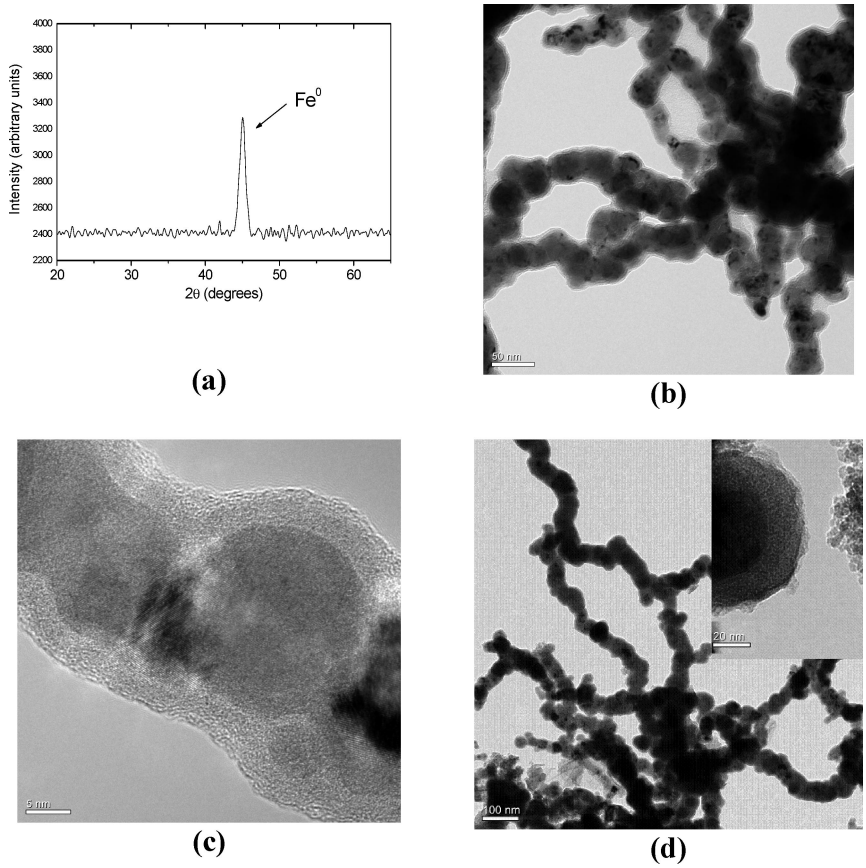

Figure 1. (a) XRD pattern of nZVI; (b,c) typical TEM images of nZVI; and (d) TEM image of nZVI aged for six months. The inset in the figure shows the propagation of the oxide layer.

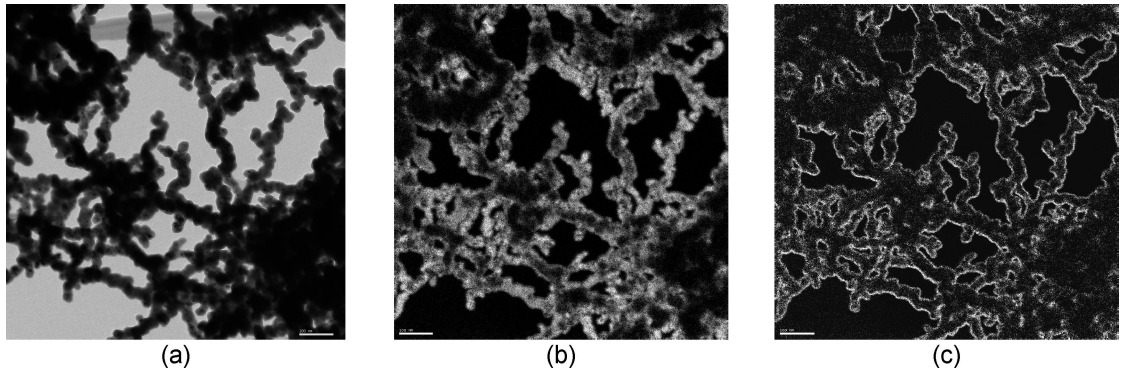

Figure 2. EELS images of a nZVI sample: (a) overall map, (b) Fe^0 map, and (c) O map.

divalent ionic form. Between pH 7 and 9.5, cationic species like $Cu(OH)^+$, $Cu_2(OH)_2^{2+}$, and $Cu_3(OH)_4^{2+}$ will be dominating. Beyond this, $Cu(OH)_2$ and the anionic species $Cu(OH)_3^-$ and $Cu(OH)_4^{2-}$ become increasingly effective. The initial and final pH values at different initial concentrations obtained in this study are given in Table 1. Within the given pH ranges and in light of the speciation analysis, copper ions are expected to possess the divalent form during the experiments.

3.2. Characterization of nZVI. An XRD pattern of freshly synthesized nZVI is shown in Figure 1a. Iron nanoparticles appear in Fe^0 state, as demonstrated by the basic reflection at 44.9°. Typical TEM images of nZVI are shown in parts b and c of Figure 1. The nZVI particles appear in the characteristic chainlike structure, with the size of individual particles predominantly ranging within 20−60 nm. The chainlike morphology of nZVI is attributed to the strong magnetic dipole−dipole attractions between the individual nanoparticles.[5] As is known, the exposure of nZVI to oxygen results in the development of an iron oxide layer, leading to a core−shell structure of the iron nanoparticles in which the core preserves the Fe^0 nature.[2,5,9,16,17] As further evidence of the core−shell structure, the nZVI samples were also analyzed using electron energy loss spectroscopy (EELS). This analysis aimed at imaging the distribution of Fe and O in the structure of the nanoparticles aggregates. The elemental maps given in Figure 2 distinctly reveal that oxygen is present in the exterior parts of the nanoparticles, forming oxide layers that surround the Fe^0 cores.

It is proposed that the oxide layer, which is about 3−5 nm thick, protects the core of the particles against further oxidation and provides a means for the transport of mass and charge across it.[5,8−10] In the HR-TEM images, while high-resolution lattice fringes appeared in the core, indicating the presence of a crystalline Fe^0 phase, such fringes were not observed in oxide images, suggesting that the iron-oxide shell is amorphous, as

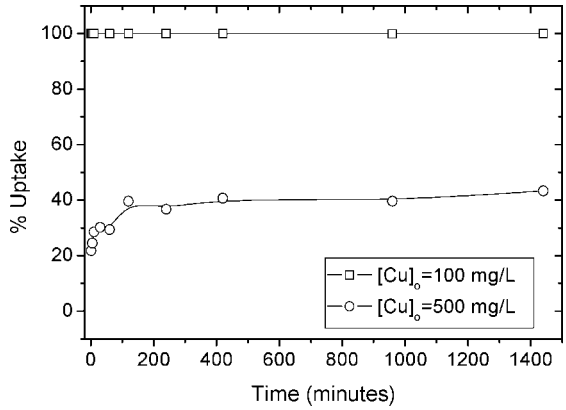

Figure 3. Variation of the % uptake of Cu^{2+} ions on nZVI with the time of contact.

also reported in earlier findings.[3] In line with the previous reports, our HR-TEM investigations showed that the oxide layer of nZVI particles did not exceed 5 nm thickness even after 8 weeks of preparation. Successive XRD analyses of the samples stored under ambient conditions showed a slow development (much slower than would normally be expected in iron powder) of iron oxides, primarily in the forms of Fe_3O_4 and γ-Fe_2O_3. A TEM image of an nZVI sample that was stored under normal conditions for about 6 months is shown in Figure 1d. In general, iron nanoparticles retain their chainlike morphology with the thickness of the oxide layer showing variation within 5−10 nm and occasionally appearing to exceed 10 nm, as shown in the figure inset.

3.3. Results of Uptake Experiments. The uptake experiments were started by investigating the time required for Cu^{2+} ions to reach equilibrium on nZVI. These experiments were performed at the initial concentrations of 100.0 and 500.0 mg/L for contact periods ranging from 1 min up to 24 h. The variation of the adsorbed amount of Cu^{2+} for the two concentrations is shown in Figure 3. The extent of removal is expressed in terms of % uptake, calculated using the following equation:

$$\%\ \text{uptake} = \frac{[\text{Cu}]_o - [\text{Cu}]_l}{[\text{Cu}]_o} \times 100\%$$

Here, $[Cu]_o$ stands for the initial concentration of Cu^{2+} ions, and $[Cu]_l$ is their concentration after the given time of contact. The uptake appears to be almost instantaneous at the initial concentration of 100.0 mg/L, with complete removal of Cu^{2+} ions being achieved after 1 min of shaking, while <3 h are required to achieve equilibrium at the initial concentration of 500.0 mg/L, with an approximate equilibrium uptake of 40%. Thus, the shaking period in the other experiments was fixed at 4 h.

The results of the experiments used to reveal the effect of initial concentration on the uptake of Cu^{2+} on nZVI are presented in Figure 4. The figure contains the uptake isotherm in addition to a bar diagram that shows the variation in % uptake with initial Cu^{2+} concentration. The isotherm appears to be of L-type in which a plateau of saturation is approached at higher concentration. The inset in the figure demonstrates that, up to the initial concentrations of 100.0 mg/L, a complete removal appears to be achieved. Beyond this concentration, a gradual decrease in the uptake capacity of the nZVI takes place, with less than one-half of the ions being removed at the initial Cu^{2+} concentrations of 500.0 mg/L. Further experiments showed that, at such a high concentration of Cu^{2+}, the extent of uptake can be enhanced by increasing the dose of nZVI. The results

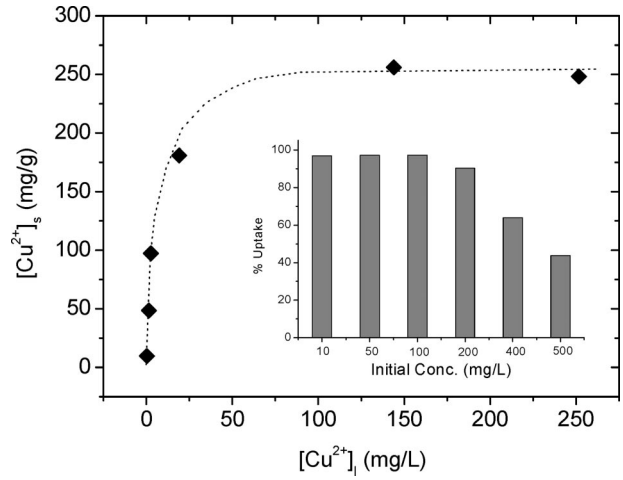

Figure 4. Isotherm of uptake of Cu^{2+} ions on nZVI. The inset in the figure shows the variation of % uptake of Cu^{2+} with the initial concentration.

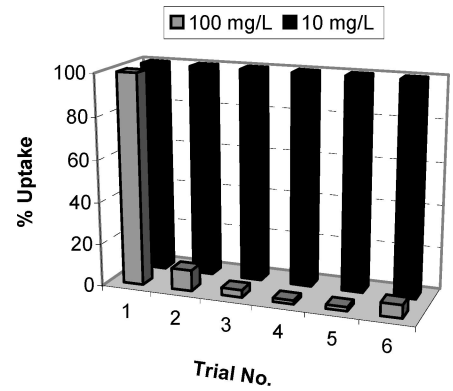

Figure 5. Variation of the % uptake of Cu^{2+} ions on nZVI with the number of successive applications of the sorbent sample at the initial concentrations of 10.0 and 100.0 mg/L.

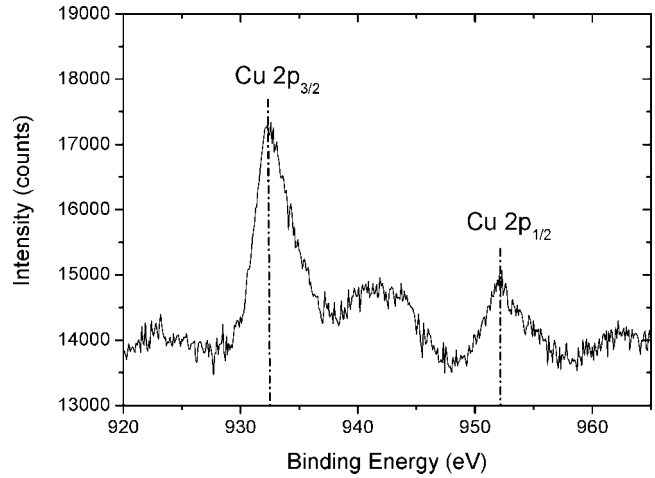

Figure 6. XPS spectrum showing Cu $2p_{3/2}$ lines on iron nanoparticles.

presented in Table 2 show that almost a complete removal of Cu^{2+} at the initial concentration of 500.0 mg/L could be achieved when the amount of nZVI was tripled. Within the studied concentration range, as shown by the uptake isotherm, the uptake capacity is around 250 mg/(g of nZVI). Here it must be noted that, as Cu^{2+} solutions were prepared from $Cu(NO_3)_2 \cdot {}_2H_2O$ salt, it seems reasonable to assume that part of the nZVI reactivity was used up in the reduction of NO_3^- ions. The capability of nZVI toward rapid and effective dinitrification was reported earlier.[15,17]

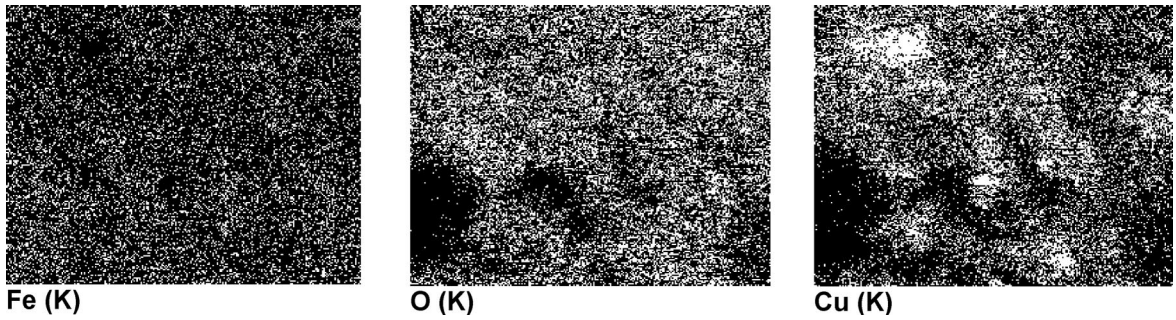

Figure 7. EDX mapping images (K lines) of the surface of iron nanoparticles after Cu^{2+} uptake: (a) Fe, (b) O, and (c) Cu.

This value seems to be much larger than most of the uptake capacities reported for Cu^{2+} removal by various sorbents, as can be seen from Table 3 in which the uptake capacities of different sorbents are compared. Here it should be stressed that the values given in the table originate from different studies in which the experimental conditions might not totally match those applied in this study and, as such, that the comparison made here aims at showing the high uptake potential of iron nanoparticles rather than establishing a priority scale among different sorbents.

The effect of repetitive loading of Cu^{2+} on the reactivity of nZVI was also tested. In each of these experiments, the same nZVI sample was repeatedly exposed to fresh aliquots of Cu^{2+} solutions for six successive trials, each lasting for 45 min. The obtained results are given in Figure 5. It is seen that, while the reactivity of nZVI deteriorated following the first round of mixing at the initial Cu^{2+} concentration of 100.0 mg/L, the same nZVI sample was very successful in retarding the Cu^{2+} ions completely at the initial concentration of 10.0 mg/L for all the studied successive trials. XRD analysis of the iron samples after uptake of Cu^{2+} ions indicated extensive oxidation of these samples as a result of exposure to aqueous solution. The oxidation products included Fe_3O_4 and Fe_2O_3, in addition to FeOOH. However, the experiments on repetitive loading indicated that, unless very high metallic concentrations are present, iron nanoparticles do not lose their reactivity toward Cu^{2+} ions even after several applications.

nZVI was tested for the removal of Cu^{2+} ions from simulated industrial estate wastewater. The composition of the simulated wastewater is provided in Table 4.[24] The results of the experiments in which 50 mL solution portions were contacted with 0.05 g of nZVI indicated that the final Cu^{2+} concentration at the end of the 4 h contact period was <0.1 mg/L, with a corresponding uptake that exceeds 99.5%.

In another set of experiments, nZVI was tested for the removal of Cu^{2+} ions prepared at initial concentrations of 10.0, 25.0, 50.0, and 100.0 mg/L in tap water of the İzmir Institute of Technology, which possesses a very hard nature (hardness index $\approx$ 5.7 g of $CaCO_3$ in 1 L of water). According to multiple ICP-AES results, the initial concentrations of Mg and Ca are 26 and 200 mg/L, respectively. The elemental concentrations obtained at the end of the uptake experiments are provided in Table 5. Even in such a hard matrix, an almost complete removal of Cu^{2+} is achieved at all concentrations. Meanwhile, a partial removal of Ca and Mg appeared to take place as well. Table 5 includes also the concentration of Fe in the liquid phases following the uptake process at different Cu^{2+} concentrations. Not much information is available in the literature about the fate of iron ions following the redox step in the course of uptake. The measurements performed in the relevant experiments indicated minimal concentrations of the element in the solution at the end of uptake; however, more experiments are still required to get a clearer picture on this issue.

3.4. Uptake Mechanism. Literature resources suggest that the uptake mechanism of metal ions by zero-valent iron is dependent mainly on the standard reduction potential and chemical speciation of the adsorbate ion under the operating pH. Earlier studies indicate that ions with standard reduction potential larger enough than that of Fe^{2+} are fixed on nZVI via an oxidation−reduction reaction in which Fe^0 behaves as a reducing agent.[7,10] The standard reduction potential of Cu^{2+} (+0.34 V, 298 K) is well above that of Fe^{2+} (−0.44 V, 298 K), and consequently, the uptake of Cu^{2+} ions would be expected to primarily take place via a redox mechanism. As shown in Figure 6, our XPS investigations indicated that Cu $2p_{3/2}$ lines are centered at a binding energy of 932.3 ± 0.1 eV. In literature, the binding energy of metallic copper, Cu^0, is frequently reported for the Cu $2p_{3/2}$ line at 932.6 ± 0.2 eV.[25,26] Meanwhile, the binding energy reported for Cu^+ in Cu_2O is also very similar to that of the metal and is reported to be centered at 932.4 ± 0.3 eV.[27] However, by calculating the Auger parameter, it is possible to determine the valence state of the Cu under analysis. The calculated Auger parameter indicated that the recorded signal was derived mainly from Cu^+ rather than Cu^0. This result was also confirmed by XRD patterns recorded for iron nanoparticles at the end of the uptake process. XRD analysis showed the appearance of more intense cuprite, Cu_2O, signals compared to metallic copper, Cu^0, signals. These results agree in part with those reported recently by Li and Zhang,[10] who suggested that Cu^{2+} ions are reduced to Cu^0 upon exposure to nZVI. However, the results are in agreement with the finding of an earlier study in which ZVI in the scrap form was employed as an adsorbent of aqueous Cu^{2+} ions.[14]

The distribution of Cu on the surface of iron nanoparticles was analyzed using EDX analysis. The mapping images for Fe (K), O (K), and Cu (K) are demonstrated in Figure 7. Most of the signals of Cu are seen to be associated with those of O, likely originating from Cu_2O. Comparatively, a smaller fraction of Cu appears with higher intensity in regions that contain weak O signals, probably corresponding to regions where Cu^0 is present.

The above findings confirm that the primary uptake mechanism is of redox type. The corresponding redox reactions, balanced by the standard redox method in acidic media, might be written as follows:

$$Fe^0 + Cu^{2+} \rightarrow Fe^{2+} + Cu^0$$

$$Fe^0 + 2Cu^{2+} + H_2O \rightarrow Fe^{2+} + Cu_2O + 2H^+$$

In addition, the recorded Cu 2p lines were asymmetric to the high binding energy side, indicating that complete Cu reduction had not occurred and that some small portion could have remained in a Cu^{2+} state.

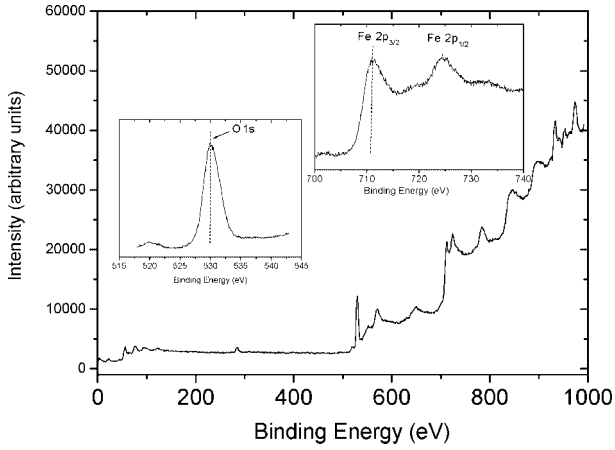

Figure 8. Typical wide XPS spectrum for Fe nanoparticles after the uptake of Cu^{2+} ions. The insets correspond to O 1s and Fe 2p photoelectron profiles in the spectrum.

Generally speaking, the availability of FeOOH groups at the solution−iron interface suggested previously in literature sources, e.g., ref 16, and also confirmed by our XRD and XPS analysis, might give rise to some contribution of surface complexation to the uptake mechanism depending on the metallic ion under investigation. A typical wide-scan XPS spectrum for Fe nanoparticles after the uptake of Cu^{2+} ions is given in Figure 8. Two insets are provided in the figure for O 1s and Fe 2p photoelectron profiles in the spectrum. The O 1s peak is centered at 530.0 ± 0.1 eV and is slightly asymmetric to the high binding energy side. Curve fitting of the O 1s profile indicated that the predominant signal contribution was derived from O^{2-} in metal oxides with a minor contribution (14% by area) from OH^-, in solid hydroxide phases and attributed to FeO(OH). The recorded Fe 2p photoelectron profiles were typical of that previously reported for Fe in hematite,[27] with the Fe $2p_{3/2}$ line centered at 711 ± 0.1 eV binding energy.

The extent of surface complexation is dependent on the isoelectric point (IEP) of the surface of iron nanoparticles. Our measurements of zeta potential of the iron nanoparticles were in agreement with previously reported values[16] and showed that the IEP occurred near pH = 8.1−8.2. Taking into consideration that the pH range of our experiments (as reported earlier in this text) was below the given value of IEP, the contribution of surface complexation in the uptake of Cu^{2+} ions seems to be insignificant. As is known, such a contribution is related with the protonation/deprotonation behavior of the surface groups, which is in turn dependent on the operating pH. In order to test this, a set of experiments was performed in which the pH of the medium was adjusted to 3.0, 5.0, 7.0, 9.0, and 11.0 at the initial Cu^{2+} concentration of 50.0 mg/L. The results indicated only minimal differences, with the uptake varying within 99.5−99.9% across the investigated pH range, verifying that the uptake process is mainly of a redox nature.

4. Conclusions

The conducted batch experiments under various conditions indicate that nZVI has fast kinetics and superior uptake ability toward Cu^{2+} ions over the range of concentrations 10.0−200.0 mg/L. The sorbent was seen to undergo serious oxidation upon contact with aqueous solution. However, high removal capabilities were still obtained in repetitive applications at lower concentrations. XPS and XRD investigations suggested that Cu^{2+} is reduced to Cu^+ (in the form of Cu_2O) and, to a lesser extent, to metallic copper, Cu^0. Further experiments are required to investigate the fate of Fe^{2+} ions that are expected to form in the course of the redox process.

Acknowledgment

This study was sponsored by the "2006 İYTE 13" fund provided by the İzmir Institute of Technology (İZTECH). The authors thank the Center of Materials Research at İZTECH for the help in SEM/EDX and BET−N_2 analysis.

Literature Cited

(1) Tratnyek, P. G.; Johnson, R. L. Nanotechnologies for Environmental Cleanup. *Nanotoday* **2006**, *1*, 44.

(2) Zhang, W.-X. Nanoscale Iron Particles for Environmental Remediation: An Overview. *J. Nanopart Res.* **2003**, *5*, 323.

(3) Nurmi, J. T.; Tratnyek, P. G.; Sarathy, V.; Bear, D. R.; Amonette, J. E.; Peacher, K.; Wang, C.; Linehan, J. C.; Matson, D. W.; Penn, R. L.; Driessen, M. D. Characterization and Properties of Metallic Iron Nanoparticles: Spectroscopy, Electrochemistry, and Kinetics. *Environ. Sci. Technol.* **2005**, *39*, 1221.

(4) Huber, D. L. Synthesis, Properties, and Applications of Iron Nanoparticles. *Small* **2005**, *1*, 482.

(5) Li, L.; Fan, M.; Brown, R. C.; Leeuwen, J. V.; Wang, J.; Wang, W.; Song, Y.; Zhang, P. Synthesis, Properties, and Environmental Applications of Nanoscale Iron-Based Materials: A Review. *Crit. Rev. Environ. Sci. Technol.* **2006**, *36*, 405.

(6) Ponder, S. M.; Darab, J. G.; Mallouk, T. E. Remediation of Cr(VI) and Pb(II) Aqueous Solutions Using Nanoscale Zero-Valent Iron. *Environ. Sci. Technol.* **2000**, *34*, 2564.

(7) Li, X. Q.; Zhang, W.-X. Iron Nanoparticles: The Core-Shell Structure and Unique Properties for Ni(II) Sequestration. *Langmuir* **2006**, *22*, 4638.

(8) Kanel, S. R.; Manning, B.; Charlet, L.; Choi, H. Removal of Arsenic(III) From Groundwater by Nanoscale Zero-Valent Iron. *Environ. Sci. Technol.* **2005**, *39*, 1291.

(9) Kanel, S. R.; Greneche, J. M.; Choi, H. Arsenic(V) Removal from Groundwater Using Nano Scale Zero-Valent Iron as a Colloidal Reactive Barrier Material. *Environ. Sci. Technol.* **2006**, *40*, 2045.

(10) Li, X.-Q.; Zhang, W.-X. Sequestration of Metal Cations with Zerovalent Iron Nanoparticles - A study with High Resolution X-Ray Photoelectron Spectroscopy (HR-XPS). *J. Phys. Chem. C* **2007**, *111*, 6939.

(11) Çelebi, O.; Üzüm, Ç.; Shahwan, T.; Erten, H. N. A Radiotracer Study of the Adsorption Behavior of Aqueous Ba^{2+} Ions on Nanoparticles of Zero-Valent Iron. *J. Hazard. Mater.* **2007**, *148*, 761.

(12) Üzüm, Ç.; Shahwan, T.; Eroğlu, A. E.; Lieberwirth, I.; Scott, T. B.; Hallam, K. R. Application of Zero-Valent Iron Nanoparticles for the Removal of Aqueous Co^{2+} Ions Under Various Experimental Conditions. Chem. Eng. J. **2008**, DOI: 10.1016/j.cej.2008.01.024.

(13) Komnitsas, K.; Bartzas, G.; Fytas, K.; Paspaliaris, I. Long-Term Efficiency and Kinetic Evaluation of ZVI Barriers During Clean-Up of Copper Containing Solutions. *Miner. Eng.* **2007**, *20*, 1200.

(14) Rangsivek, R.; Jekel, M. R. Removal of Dissolved Metals by Zero-Valent Iron (ZVI): Kinetics, Equilibria, Processes and Implications for Stormwater Runoff Treatment. *Water Res.* **2005**, *39*, 4153.

(15) Wang, W.; Jin, Z.-H.; Li, T.-L.; Zhang, H.; Gao, S. Preparation of Spherical Iron Nanoclusters in Ethanol−Water Solution for Nitrate Removal. *Chemosphere* **2006**, *65*, 1396.

(16) Sun, Y.; Li, X.; Cao, J.; Zhang, W.; Wang, H. P. Characterization of Zero-Valent Iron Nanoparticles. *Adv. Colloid Interface Sci.* **2006**, *120*, 47.

(17) Sohn, K.; Kang, S. W.; Ahn, S.; Woo, M.; Yang, S.-K. Fe(0) Nanoparticles for Nitrate Reduction: Stability, Reactivity, and Transformation. *Environ. Sci. Technol.* **2006**, *40*, 5514.

(18) Banerjee, S. S.; Chen, D.-H. Fast Removal of Copper Ions by Gum Arabic Modified Magnetic Nano-Adsorbent. *J. Hazard. Mater.* **2007**, *147*, 792.

(19) Kumar, G. P.; Kumar, P. A.; Chakraborty, S.; Ray, M. Uptake and Desorption of Copper Ion Using Functionalized Polymer Coated Silica Gel in Aqueous Environment. *Sep. Purif. Technol.* **2007**, *57*, 47.

(20) Chiron, N.; Guilet, R.; Deydier, E. Adsorption of Cu(II) and Pb(II) Onto a Grafted Silica: Isotherms and Kinetic Models. *Water Res.* **2003**, *37*, 3079.

(21) Gupta, V. K. Equilibrium Uptake, Sorption Dynamics, Process Development, and Column Operations for the Removal of Copper and Nickel from Aqueous Solution and Wastewater Using Activated Slag, a Low-Cost Adsorbent. *Ind. Eng. Chem. Res.* **1998**, *37*, 192.

(22) Farajzadeh, M. A.; Monji, A. B. Adsorption Characteristics of Wheat Bran Towards Heavy Metal Cations. *Sep. Purif. Technol.* **2004**, *38*, 197.

(23) Gupta, V. K.; Rastogi, A.; Saini, V. K.; Jain, N. Biosorption of Copper(II) From Aqueous Solutions by *Spirogyra* species. *J. Colloid Interface Sci.* **2006**, *296*, 59.

(24) Sirianuntapiboon, S.; Hangsrisuwan, T. Removal of Zn^{2+} and Cu^{2+} by a Sequencing Batch Reactor (SBR) System. *Bioresour. Technol.* **2007**, *98*, 808.

(25) Gaarenstroom, S. W.; Winograd, N. Initial and Final State Effects in ESCA Spectra of Cadmium and Silver Oxides. *J. Chem. Phys.* **1977**, *67*, 3500.

(26) Wagner C. D.; Riggs W. M.; Davis L. E.; Moulder J. F.; Muilenberg G. E. *Handbook of X-Ray Photoelectron Spectroscopy*; Perkin-Elmer Corporation, Physical Electronics Division: Eden Prairie, MN, 1979.

(27) Wagner, C. D. Chemical Shifts of Auger Lines, and the Auger Parameter. *Faraday Discuss. Chem. Soc.* **1975**, *60*, 291.

Received for review January 17, 2008
Revised manuscript received April 18, 2008
Accepted May 4, 2008

IE800081S